Proceedings of the 26th International Conference on
Port and Ocean Engineering under Arctic Conditions
June 14-18, 2021, Moscow, Russia

Comparison of Full-scale and DEM simulation Data on Ice Loads Due to Floe Fields on a Ship Hull

Arttu Polojärvi[1], Hanyang Gong[1], Jukka Tuhkuri[1]
[1]Aalto University, School of Engineering, Department of Mechanical Engineering, P.O. Box 14100, FI-00076 Aalto, Finland

ABSTRACT

Ship passage through an ice floe field was simulated with 3D discrete element method (DEM). In the simulations, the ship traveled through a 2 km long ice floe field with constant velocity, while the local ice loads, due to the ship contacting with the ice floes, were gauged. Ice floes were simplified in their shape, they were rigid and not allowed to fracture. The ice floe field properties, such as ice floe thickness, average floe size and ice coverage, were varied. The simulated local ice loads were compared to those measured in full-scale.

KEY WORDS: discrete element method, numerical ice mechanics, ice loads

INTRODUCTION

The ships operating on ice covered seas often encounter floe fields, sea areas with partial ice cover consisting of individual ice floes of different sizes and shapes. Estimating the ice loads due to ship-floe collisions is crucial for safety, yet the understanding of these local loads is insufficient. This paper aims to increase this understanding by focusing on discrete element method (DEM) simulations on ship passage through an ice floe field, and especially on the comparison of the local ice loads simulated and measured in similar ice conditions. DEM suits well for the study presented, as it enables modeling individual ice floes and their interaction with each other and the ship. The technique has been used ice mechanics since the mid-80's (Tuhkuri and Polojärvi, 2018). DEM and other numerical tools capable of describing numerous individual ice features have been used in several studies related to the ice resistance of ships due to level ice, ice floes or ice rubble (Lubbad and Løset, 2011; Metrikin and Løset, 2013; Gong, Polojärvi and Tuhkuri, 2019; van den Berg, Lubbad and Løset, 2020; Yang *et al.*, 2021), while less attention has been given on the simulation of local loads in ice floe fields (Daley *et al.*, 2014; Kim *et al.*, 2019).
This paper focuses on comparing the results from 3D DEM simulations to full-scale measurements performed onboard S.A. Agulhas II. Section 2 describes the simulations, the properties of the modeled floe fields and the full-scale measurements used for comparison. Section 3 presents the simulation results and compares them to full-scale data. Section 4 concludes the paper. The work summarizes part of the study by Polojärvi *et al.* (2021).

METHODS

Simulations

The simulations were performed using the inhouse 3D DEM code of Aalto University Ice Mechanics Group. The current version of the code is similar to the one that has been used to model ice rubble punch through tests and ship passage through ice rubble piles (Polojärvi and Tuhkuri, 2009; Gong, Polojärvi and Tuhkuri, 2019). Figures 1 and 2 show snapshots from the simulations and demonstrate, how the ice floes in the simulation interact through contacts with each other and the ship. The interaction leads to contact forces, which result into floe translation, rotation, and rafting. Floe deformation or fracture were not modeled.

The floe-to-floe and floe-to-ship interaction occurs through contacts, which lead to contact forces. The normal contact forces are calculated based on elastic-viscous-plastic contact force model. Calculation of the elastic normal contact force is outlined by Feng and Owen (2004) and Feng *et al.* (2012), while viscous and plastic load components were determined as described by Hopkins (1992). Tangential contact forces were calculated by using an incremental tangential contact force model with Coulomb friction (Hopkins, 1992). The simulation tool describes local crushing at contacts. The magnitude of local crushing is governed by a plastic limit, which makes the maximum contact force depended of the area of contact, or in other words, the load patch. There are no new ice fragments created in local crushing. Parameterization of the contact force model is based on material properties of ice and performed following Chen (2012). Water is accounted for by buoyant force, a simple model for pressure drag, and by using added mass for the ice floes. The parameters used in the simulations are described in Table 1.

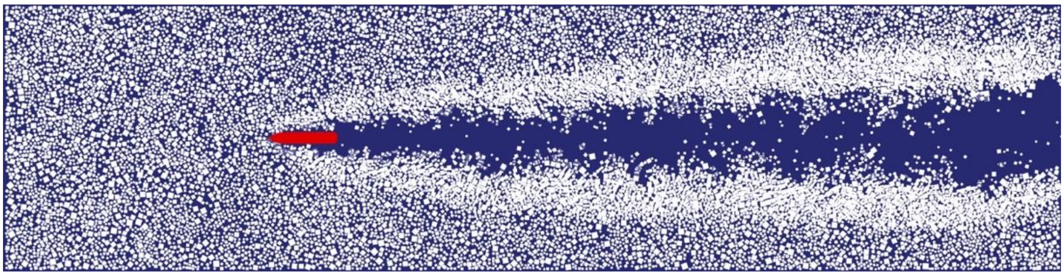

Figure 1. Snapshot from a simulation with ice floe field consisting of 14329 rectangular floes of size 5…15 m and thickness 0.5 m. The floe field has ice concentration of 50 % and its dimensions are 0.5 km × 2.0 km. Ship is moving with constant velocity of 1 m/s.

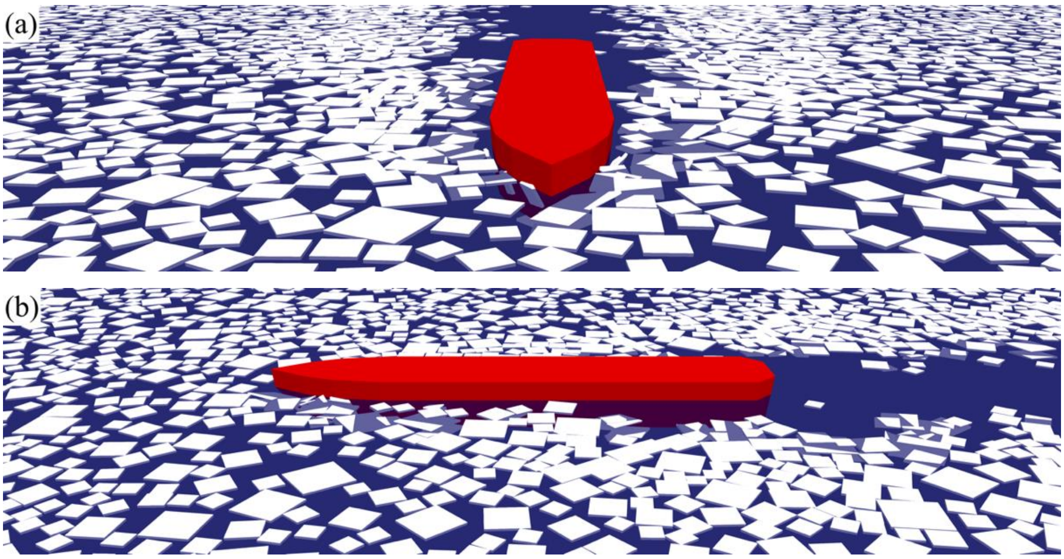

Figure 2. Simulation snapshots from (a) the front and (b) the side of the showing rotated and rafted, 0.5 m thick, ice floes around the ship hull and the open channel behind the ship.

Table 1. Main parameters of the simulations.

Parameter		Value
General	time step	2e-4 s
	gravitational acceleration	9.81 m/s^2
	drag coefficient	1
	water density	1010 kg/m^3
	simulated period	2000 s
Ice floes*	effective modulus	1 GPa
	Poisson's ratio	0.3
	density	920 kg/m^3
	damping ratio	0.75
	friction coefficient	0.5
	plastic limit	1 MPa
Ship hull	velocity	1 m/s
	bow length	~30 m
	breadth	22 m

*Table 2 presents data on floe sizes and thicknesses

The modeled hull had the same main dimensions and hull angles than S.A. Agulhas II, but its geometry was simpler, formed with flat planes. The simulated ship moved on a straight line through the floe field with a constant velocity of 1 m/s, while the other degrees of freedom of the ship were fixed. As the floe field was 2.0 km in length, the total duration of a simulation was 2000 s. The simulation tool used is parallelized and, depending on the case, the simulations were performed by using 8…32 cores. Maximum wall clock time for an individual simulation was a few hours.

Floe field properties

Table 2 summarizes the properties of the simulated floe fields, while Figure 3 illustrates their appearance. The floe fields differed by the floe size, thickness, and ice concentration. Two different size ranges, 5 … 15 m and 15 … 30 m, were used and, for both size ranges, the size distribution followed that presented by Rothrock and Thorndike (1984). The ice concentrations used were 50 % and 80 %, the latter chosen after the upper limit for ice floe packing in a single layer; at higher concentrations ice floes start rafting when a floe field is compacted (Hopkins and Tuhkuri, 1999). The individual floes were here rectangular, even if the used simulation tool does not limit the shape of the modeled ice features; the sizes above refer to the diagonal of the rectangular floe. The floe fields had dimensions of 0.5 km × 2.0 km (width × length), while the simulation domain was unbounded, that is, there was no constraints on the floe motion on the boundaries of the floe fields. Simulations with floe fields of width 1.0 km were also performed with no change in the results.

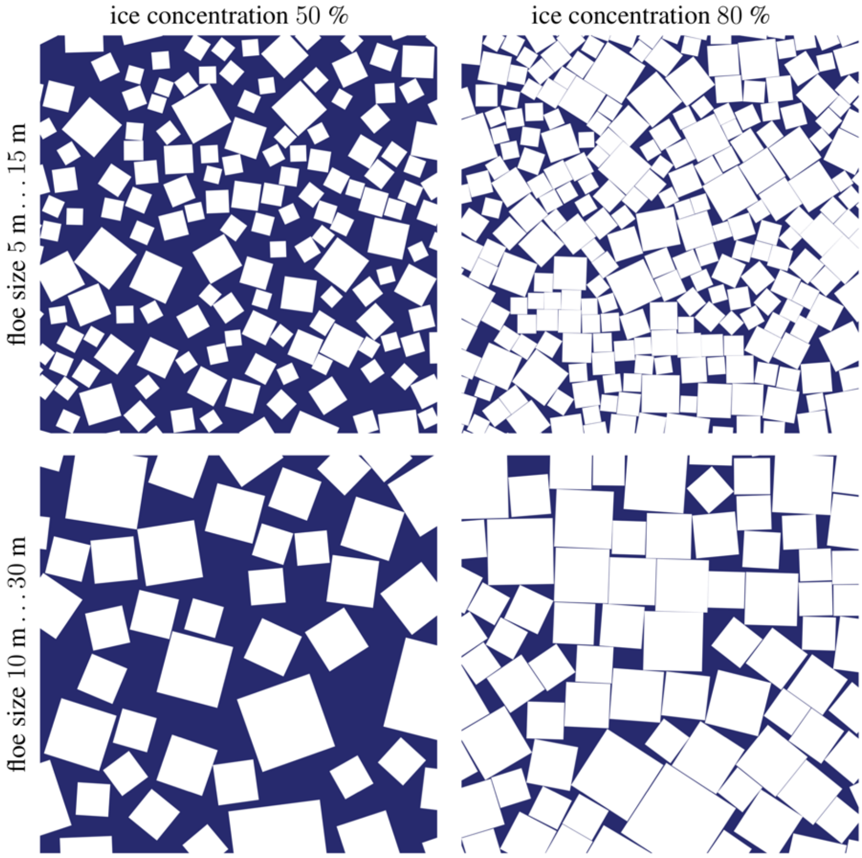

Figure 3. Floe fields with different properties: Floe size increases from top to bottom and concentration from left to right. Each picture shows an area of 100 m × 100 m. The properties varied in this work were the floe size, ice thickness and ice concentration (Table 2).

Table 2. Summary of the floe field properties in DEM simulations. h is the floe thickness, c the ice concentration, d_{min} and d_{max} the minimum and maximum diameter of the floes, respectively. Last column shows the number of floes in each simulation.

ID	h [m]	c [%]	$d_{min}...d_{max}$ [m]	n of floes
S01	1	50	5...15	14483
S02	1	80	5...15	22860
S03	1	50	10...30	3583
S04	1	80	10...30	5788
S05	0.5	50	5...15	14329
S06	0.5	80	5...15	22794
S07	0.5	50	10...30	3586
S08	0.5	80	10...30	5760

Full-scale data

The local ice loads obtained from the simulations are compared to full-scale data from S.A. Agulhas II (Figure 4). Measurements on board S.A. Agulhas II have been performed since 2012 and have included ice loads, ship navigational and operational data, and ice conditions (Suominen and Kujala, 2015). The loads measured with an instrumented panel at bow, at the waterline, were used here—in the simulations the ice loads applied on the hull area where the panel was located were recorded. The instrumented panel had dimensions 0.4 m × 1.175 m (width × height) and area A_{ip} = 0.47 m^2. The local ice load (P), measured in full-scale and recorded in the simulations, was acting normal to the ship hull. Table 3 summarizes the main properties of the South Atlantic floe fields used here as case study areas.

Occasionally in the simulations the area of contact, or the load patch, was larger than the area of the panel, $A > A_{ip}$. In such cases the resultant load recorded was multiplied by factor A_{ip} /A. This is because the panel capacity in real life would have been exceeded: The panel would not have measured the total load in a case the load patch was larger than the panel area. Since the plastic limit for the simulated floes is known, the upper limit for the load in the simulations can be defined: With plastic limit 1 MPa (Table 1), the upper limit for the ice load in the simulations is 470 kN, the product of the plastic limit and the panel area.

RESULTS AND ANALYSIS

Figures 5 presents an ice load record (P-δ) from a full-scale measurement and a simulation. It can be seen that both the full-scale and simulation data show similar features. In both cases P-records presented show long periods of negligible load interrupted by transient peaks. The full-scale data, in addition, show noise of small amplitude and near-zero mean value. The noise is due to waves and other hydrodynamic effects. The simulation data does not include the noise, since no hydrodynamical effects acting on the ship hull were modeled. Towards the end of the simulation, the load reaches the limit of 470 kN (Section 2.1), also indicated in the figure. Peak loads could be due to impact of individual floes and floe accumulations in front of the ship.

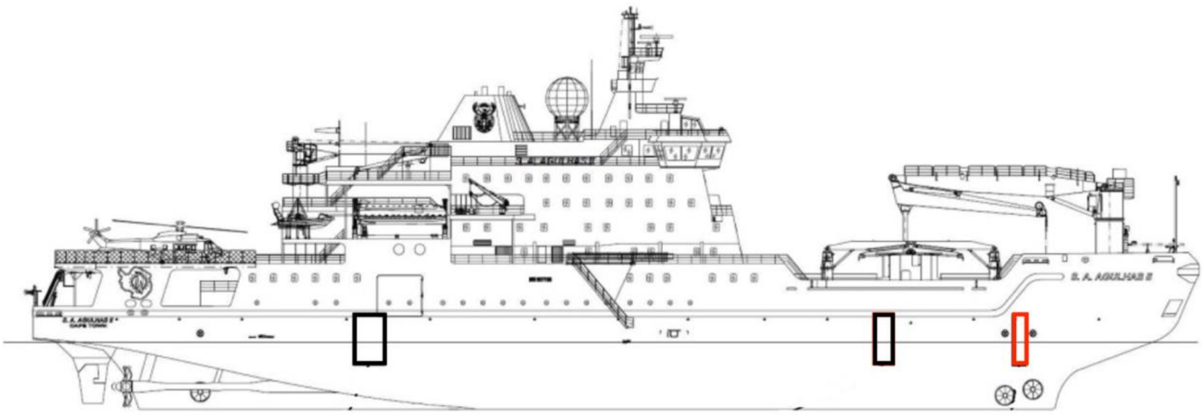

Figure 4. S.A. Agulhas II. The three rectangles on the hull show locations where the ice loads are measured (Suominen and Kujala, 2015). The loads from the simulations were compared to the loads measured with the panel (red) at the bow.

Table 3. Summary of the South Atlantic floe field properties in full-scale measurements. h is the floe thickness, c the ice concentration, d_{min} and d_{max} the minimum and maximum diameter of the floes, respectively, and δ_{tot} the total length of ship travel.

ID	h [m]	c [%]	$d_{min}...d_{max}$ [m]	δ_{tot} [km]
F01	0.53	90	0...30	3.3
F02	0.56	70	50..100	2.5
F03	0.73	30	0...20	4.6
F04	0.87	30	10...30	4.2
F05	0.80	90	20...50	4.4
F06	0.72	90	20...40	4.7
F07	0.72	50	20...50	2.5
F08	1.06	70	20...40	2.0
F09	1.57	50	10...30	1.9
F10	1.30	50	0...20	4.0

Figure 5 further indicates the peak ice load events (P^p) by square markers. The values of P^p were determined from the load records by using Rayleigh separation similarly to Suominen and Kujala (2015) and Suominen *et al.* (2017). Figure 6 compares the P^p from the simulations with those from the full-scale measurements. Both data are plotted as a function of ice floe thickness (h). The figure illustrates how the mean value of P^p from the simulations is somewhat higher than what was measured in full-scale, yet the 90 % quantiles appear to be on the same range in both cases. Neither full-scale nor simulation data show dependency on h. This surprising result may be due to sampling: The instrumented panel used in the load measurements is relatively small. The statistics for the P^p data are summarized by Table 4. The maximum values show large scatter, but the values from the simulations are on the range of those measured in full-scale.

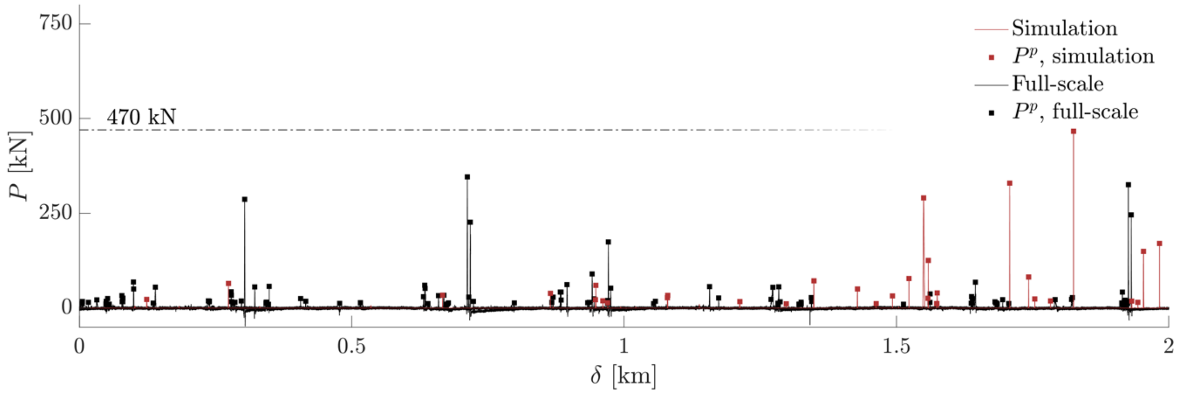

Figure 5. The ice load (P) plotted against ship penetration (δ) in the simulations and in the full-scale measurements. Peak loads (P^p) are indicated by square markers.

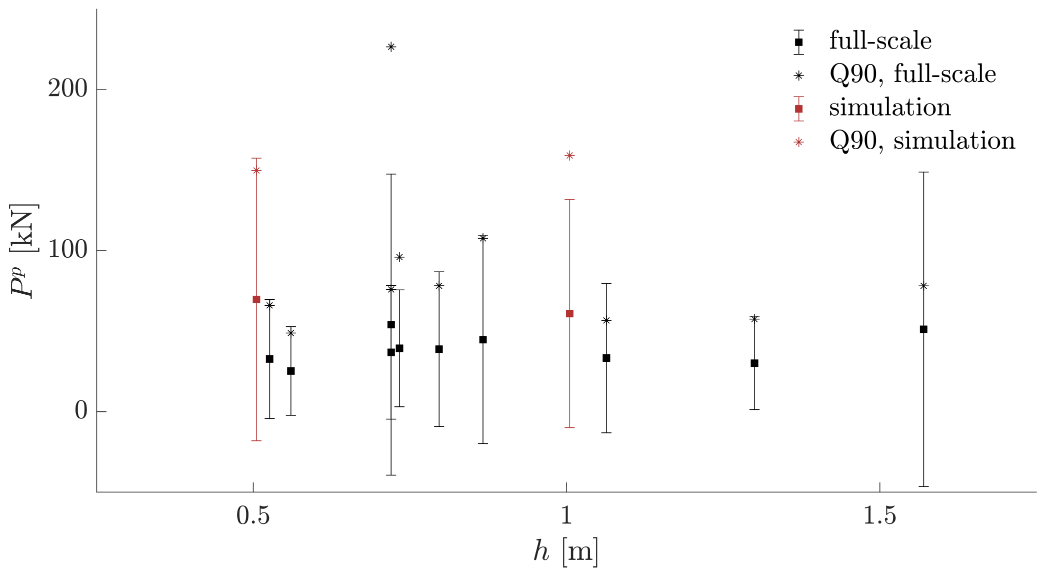

Figure 6. Peak loads (P^p) recorded in full-scale and in the simulations against floe thickness h. The figure shows the mean, standard deviation and 90 % quantile (Q90) for the P^p values. Data from all simulations with given h was combined when calculating the statistics shown.

A simple reason for the values of P^p from the simulations being somewhat higher than those measured in full-scale was that the simulated data included less P^p observations of small value than the data measured in full-scale. The full-scale P^p observations are likely to include (1) ice floe failures and (2) contacts by small ice fragments broken off the floes, neither of which were modeled. The comparison between the simulated and the full-scale data, thus, suggests that the peak loads of small and large values may stem from different sources: Small peaks are due to broken ice and large peaks due to impacts between the floes and the ship.

CONCLUSIONS

This paper focused on comparing the local ice load data, of a ship advancing in a ice floe field, as generated by using 3D DEM simulations to data on full-scale measurements. The simulations yield data, which compares fairly well with the full-scale data, yet in general the loads in the simulations are somewhat larger than those in full-scale. Here the focus was on comparison of simulation and full-scale data. Thus, topics such as the effect of floe field properties such as the ice floe shape on ice loads were not discussed. Extended version of this study can be found from Polojärvi *et al.* (2021) and includes analysis on these topics.

ACKNOWLEDGEMENTS

The financial support of the Lloyd’s Register Foundation is acknowledged with gratitude. Lloyd’s Register Foundation helps to protect life and property by supporting engineering-related education, public engagement and the application of research. Dr. Fang Li and MSc. Liangliang Lu from Aalto University are acknowledged for their work on searching for the full-scale data suitable for comparison with the simulations.

Table 4. Average (AVG), standard deviation (STD), 90 % quantile (Q90) and maximum (MAX) for the values of peak ice loads (P^p) measured in full-scale and recorded in the simulations.

	P^p			
	ID	AVG+STD [kN]	Q90 [kN]	MAX [kN]
FULL-SCALE	F01	33±37	66	301
	F02	25±28	49	158
	F03	39±36	96	184
	F04	45±65	108	429
	F05	39±48	78	443
	F06	37±41	76	328
	F07	54±94	227	398
	F08	33±46	57	326
	F09	51±98	78	598
	F10	30±29	57	170

	P^p			
	ID	AVG+STD [kN]	Q90 [kN]	MAX [kN]
SIMULATIONS	S01	68±57	103	202
	S02	55±36	99	122
	S03	47±58	154	218
	S04	72±79	147	333
	S05	75±105	171	467
	S06	64±67	137	332
	S07	310±213	470	470
	S08	99±68	161	246

REFERENCES

van den Berg, M., Lubbad, R. and Løset, S. (2020) ‘Repeatability of ice-tank tests with broken ice’, *Marine Structures*, 74, p. 102827. doi: 10.1016/j.marstruc.2020.102827.

Chen, J. (2012) *Discrete element method for 3D simulations of mechanical systems of non-spherical granular materials*. The University of Electro-Communications.

Daley, C., Alawneh, S., Peters, D. and Colbourne, B. (2014) ‘GPU-Event-Mechanics evaluation of ice impact load statistics’, in *Proceedings of the Arctic Technology Conference*, OTC Paper Number 24645.

Feng, Y. T., Han, K. and Owen, D. R. J. (2012) ‘Energy-conserving contact interaction models for arbitrarily shaped discrete elements’, *Computer Methods in Applied Mechanics and Engineering*, 205–208(1), pp. 169–177.

Feng, Y. T. and Owen, D. R. J. (2004) ‘A 2D polygon/polygon contact model: Algorithmic aspects’, *Engineering Computations*, 21(2–4), pp. 265–277.

Gong, H., Polojärvi, A. and Tuhkuri, J. (2019) ‘Discrete element simulation of the resistance of a ship in unconsolidated ridges’, *Cold Regions Science and Technology*, 167.

Hopkins, M. A. (1992) *Numerical Simulation of Systems of Multitudinous Polygonal Blocks.*

Hopkins, M.A. and Tuhkuri J. 1999. ‘Compression of floating ice fields’. *Journal of Geophysical Research*, 104 (C7): 15,815-15,825.

Kim, J-H., Kim Y., Kim, H-S. and Jeong, S-Y. (2019) ‘Numerical simulations of ice impacts on ship hull in broken ice fields’, *Ocean Engineering*, 180, pp. 162–174.

Lubbad, R. and Løset, S. (2011) ‘A numerical model for real-time simulation of ship-ice interaction’, *Cold Regions Science and Technology*, 65(2), pp. 111–127.

Metrikin, I. and Løset, S. (2013) ‘Nonsmooth 3D discrete element simulation of a drillship in discontinuous ice’, in *Proceedings of the 22nd International Conference on Port and Ocean Engineering under Arctic Conditions, POAC’13*. Espoo, Finland (electronic publication).

Polojärvi, A. *et al.* (2021) ‘3D DEM simulations on ship passage through an ice floe field: Local ice loads’, *(in review)*.

Polojärvi, A. and Tuhkuri, J. (2009) ‘3D discrete numerical modelling of ridge keel punch through tests’, *Cold Regions Science and Technology*, 56(1).

Rothrock, D. A., and Thorndike, A. S. (1984), Measuring the sea ice floe size distribution, *Journal of Geophysical Research*, 89(C4), 6477– 6486

Suominen, M. *et al.* (2017) ‘Influence of load length on short-term ice load statistics in full-scale’, *Marine Structures*, 52, pp. 153–172. doi: 10.1016/j.marstruc.2016.12.006.

Suominen, M. and Kujala, P. (2015) ‘The measured line load as a function of the load length in the Antarctic Waters’, in *Proceedings of the 23rd International Conference on Port and Ocean Engineering under Arctic Conditions, POAC*, p. (electronic publication).

Tuhkuri, J. and Polojärvi, A. (2018) ‘A review of discrete element simulation of ice-structure interaction’, *Philosophical Transactions of the Royal Society A: Mathematical, Physical and Engineering Sciences*, 376(2129).

Yang, B. *et al.* (2021) ‘Numerical estimation of ship resistance in broken ice and investigation on the effect of floe geometry’, *Marine Structures*, 75, p. 102867.